Camera and Lidar Cooperation for 3D Feature Extraction

Burtin Gabriel[1], Bonnin Patrick[2] and Malartre Florent[1]
[1]*4D-Virtualiz, 10 Allee Evariste Galois, Clermont-Ferrand, France*
[2]*LISV, Universite de Versailles St Quentin, 10-12 Avenue de l'Europe Velizy, France*

Keywords: Line Segment Detection, Algorithm Optimization, Camera-lidar Sensor Fusion, Localization, Extended Kalman Filter.

Abstract: The objective of this work is to use efficiently various sensors to create a SLAM system. This algorithm has to be fast (real-time), computationally light and efficient enough to allow the robot to navigate in the environment. Because other processes embedded require large amount of cpu-time, our objective was to use efficiently complementary sensors to obtain a fairly accurate localization with minimal computation. To reach this, we used a combination of two sensors: a 2D lidar and a camera, mounted above each other on the robot and oriented toward the same direction. The objective is to pinpoint and cross features in the camera and lidar FOV. Our optimized algorithms are based on segments detection. We decided to observe intersections between vertical lines seen with the camera and locate them in 3D with the ranges provided by the 2D lidar. First we implemented a RGB vertical line detector using RGB gradient and linking process, then a lidar data segmentation with accelerated computation and finally we used this feature detector in a Kalman filter. The final code is evaluated and validated using an advanced real-time robotic simulator and later confirmed with a real experiment.

1 INTRODUCTION

The robot of the future is built to work in the new hi-tech "factory". It is given tasks to complete in a cluttered, yet structured and human environment. To complete these tasks, the robot must move between locations, with a possibility of encountering humans. We need a navigation system to able to work fast, be reliable and take advantage of the structured characteristic of the environment. This problem can be divided in sub-tasks: localization, mapping, path-planning, control and safety management. All these tasks must be performed within an embedded computation unit on the robot. This means that each task must consume computational resources as little as possible. On the other hand, the robot is moving and needs a regular update on its status. The goal is to reduce computation cost induced by each element of the navigation system. The concept of localization is to give the robot an idea of "where" it is on a map. This map can be either known previously or built during the robot evolution in the environment, also known as SLAM (simultaneous localization and mapping (Durrant-Whyte and Bailey, 2006)).

In our case, the environment is human made, composed of a flat floor, rooms with various sizes, shapes and furniture, all of them connected though hallways. This environment is likely to be an hospital, a factory or offices, thus it is populated and traveled by humans at all times. The place is neither collaborative (we don't use man-made landmarks) nor hostile (nothing is going to make an attempt at putting the robot out of action). Humans are considered as "passive" disturbance and are not likely actively trying to break the robot. Human detection and handling have yet to be done but are not part of this work; however, they have direct effects on the degrees of freedom. These two steps are indeed achieved through the analysis of sensor data provided by a camera. As we can see, one sensor is already decided. This human detection process is particularly CPU-consuming and have priority (safety is the most important task), therefore, the CPU time allowed to our algorithm is reduced. This lowered CPU time availability is a major constraint to be taken into account in the design of our localization method.

First we will have a look at previous and related work, then we will detail the vision and lidar process followed by an implementation of this feature extractor in a SLAM algorithm using an Extended Kalman

Gabriel, B., Patrick, B. and Florent, M.
Camera and Lidar Cooperation for 3D Feature Extraction.
DOI: 10.5220/0007808900230033
In *Proceedings of the 16th International Conference on Informatics in Control, Automation and Robotics (ICINCO 2019)*, pages 23-33
ISBN: 978-989-758-380-3

Filter. At last, the performances are first evaluated using an advanced real-time robotic simulator (Burtin et al., 2016), then with a real robot/sensor set-up.

2 RELATED WORK

Using segments to perform SLAM processing have been explored either with a lone lidar (Roumeliotis and Bekey, 2000), (Choi et al., 2008) or camera alone (Huang, 2008), (Lemaire and Lacroix, 2007), (Micusik and Wildenauer, 2015), (Zuo et al., 2017). SLAMs are generally split between sparse and dense vision algorithms. Sparse SLAMs are using only a few salient features in the image to compute the localization, for example the ORB-SLAM (Mur-Artal et al., 2015). Each feature is represented and stored specifically in the map to be used later as reference in the localization algorithm. These types of process only need a small percentage of the pixels from the entire image to be tracked, while dense methods use almost all the pixels. Because dense methods such as DTAM (Newcombe et al., 2011) uses every pixels from the image, users need a powerful hardware to perform all the operations in real-time. Most of the time, GPU processing is used to improve the computation speed. RGB-D (Kinect, Xtion) and depth camera sensors brought new SLAMs systems (Engelhard et al., 2011), (Schramm et al., 2018), with new approaches. They avoid the issue of initialization from unknown range for the features. Monocular cameras have the weakness to be unable, using only one frame, to obtain the distance between an object and the camera for its given pixel in the image (scale effect). LSD (Von Gioi et al., 2012) is massively used by monocular and stereo-vision SLAMs systems (Engel et al., 2014) or (Pumarola et al., 2017) but this line segment detector is too generic and extracts all segments available while processing only B&W images: the process is not optimized enough. Moreover, the RGB to B&W conversion is a potential danger of missing gradients because of the gray level conversion method. The idea to use both lidar and monocular camera has been more usually applied to mobile objects detection and tracking (Premebida et al., 2007), (Asvadi et al., 2016), (De Silva et al., 2018) but more rarely to localization itself. In our case, we will focus on the detection of vertical lines in the camera because they are commonly found and invariants regarding our environment. The common slam, using these types of features are commonly referred as "bearing" only slam (Bekris et al., 2006), they are proven effective in minimalist set-ups with simple environments (Huang, 2008), (Choi et al., 2008), (Zuo et al., 2017).

In order to extract these vertical segments in the image (which are supposed to be the projection of 3D vertical structures of the scene: doors, angles of corridors), we are looking for classical edge segmentation composed of well known steps (Nachar et al., 2014):

1. gradient computation ;
2. thinning ;
3. closing ;
4. linking ;
5. and polygonal approximation.

The gradient computation being the most time consuming step, we will detail the choice of the appropriate algorithm in this section, its adaptation and its time optimized implementation (Cabrol et al., 2005) in the next section.

The gradient computation algorithms could be classified into three categories, according to their complexity, and the size of the neighborhood:

- 2×2: Roberts (Roberts, 1965) proposed in the 60's;
- 3×3: Prewitt (Prewitt, 1970), Sobel (Sobel, 1978) and Kirsh (Kirsch, 1971) in the 70's;
- JF Canny ((Canny, 1983)) (in OpenCV), R.Deriche ((Deriche, 1987)) in the 80's.

Although better quality results are obtained by algorithms of the last category, the best compromise between the quality of results and the sum of computations, for our real-time and embedded robotic application, is given by the second one.

The principle of Prewitt and Sobel algorithms is to compute the projection of the gradient $\overrightarrow{G}$ on the axis of the image: $\overrightarrow{u_x}$ and $\overrightarrow{u_y}$ first and, then, to perform a rectangular to polar transformation to obtain:

- the gradient magnitude, which is the reflect of the transition between two regions;
- the gradient argument, which is orthogonal to the local edge direction. This information is reduced to the knowledge of direction of the neighbor pixel in the orthogonal direction of the edge for the thinning step, ie. four directions.

$$||\overrightarrow{G}|| = \sqrt{(\overrightarrow{G}.\overrightarrow{u_x})^2 + (\overrightarrow{G}.\overrightarrow{u_y})^2}$$

$$Arg(\overrightarrow{G}) = \arctan\left(\frac{\overrightarrow{G}.\overrightarrow{u_y}}{\overrightarrow{G}.\overrightarrow{u_x}}\right)$$

In order to obtain quite same results, and avoid the computations (in double floats if done without approximation) of the rectangular to polar transform, Kirh introduced two diagonal direction of projection:

$\overrightarrow{u_{45}}$ and $\overrightarrow{u_{-45}}$. Thus the gradient magnitude was approximated by the longer projection, and the argument by the Freeman code corresponding to the best projection.

$$||\vec{G}|| = Max\{|\vec{G}.\vec{u_x}|, |\vec{G}.\vec{u_y}|, |\vec{G}.\overrightarrow{u_{45}}|, |\vec{G}.\overrightarrow{u_{-45}}|\}$$

$$Arg(\vec{G}) = \begin{cases} 0, \text{ if } ||\vec{G}|| = |\vec{G}.\vec{u_x}| \\ 6, \text{ if } ||\vec{G}|| = |\vec{G}.\vec{u_y}| \\ 1, \text{ if } ||\vec{G}|| = |\vec{G}.\overrightarrow{u_{45}}| \\ 7, \text{ if } ||\vec{G}|| = |\vec{G}.\overrightarrow{u_{-45}}| \end{cases}$$

Another way, which seems to be promising, is to use *Edgels* or *Line Segment Detectors*: small edge segments are gathered into bigger ones using region growing algorithms.

3 APPROACH

The most important statement considering our hypothesis is the fact that the robot is evolving in a man-made environment, comparable to an industry (factory) or office/hospital type. We state that the robot will encounter numerous structured elements with strong vertical and horizontal lines. Considering a flat floor, we also assume that the movement is only 2D. With this new assumption and the previous one, we can narrow features to propose a sparse localization method using specific landmarks. The most invariant observable elements in the image, as explained before, are going to be the vertical lines. 3D horizontal and other more random lines would have an incidence angle due to the point of view of the camera and wouldn't be invariant in the image, thus inducing more computation to detect and track them.

The localization process is an optimized parallel pipeline able to cross data from the lidar and camera sensors (Figure: 1). Each data process is split, but synchronous to use both extracted data at the same moment during the feature extraction stage. The objective is to detect a feature and determine its 3D position in the camera frame. The camera process extracts vertical lines in the image while the lidar process does a segmentation and a time-forward prediction to match the camera's data time-stamp.

The lidar, placed horizontally on the robot, produces an horizontal plane with the successive distances measurements. Our lidar process produces, through the lidar segmentation algorithm, a set of lines representing the environment around our robot. The camera, located above the lidar, through the lines detection algorithm, extracts a set of vertical lines in the focal plane of the image. The fusion of both of these data gives us a set of 3D points in the camera frame (Figure: 2).

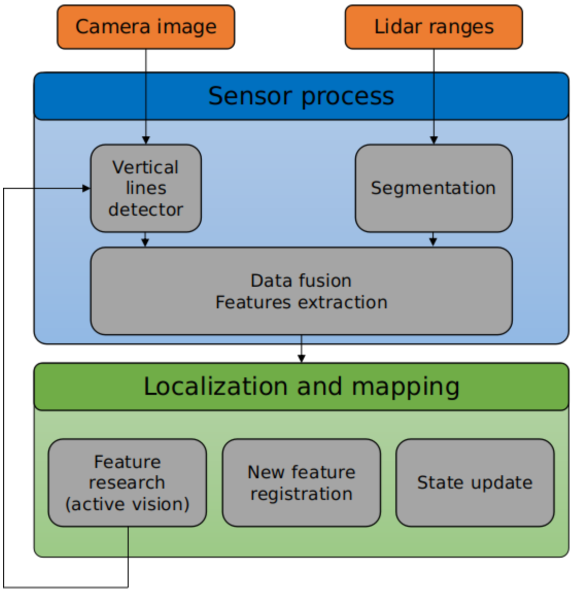

Figure 1: System overview.

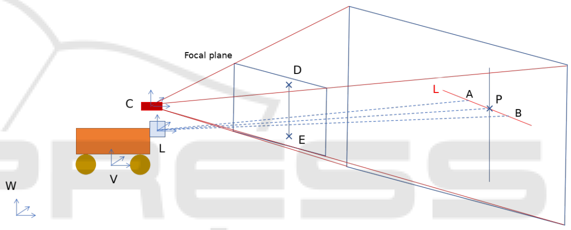

Figure 2: Feature (P) detected in the focal and lidar plane.

First we will see the optimized vertical lines detection algorithm for images processing.

Then we will develop the 3D points extraction process using the camera vertical features and the horizontal lines from the lidar process.

In the end, we will propose a SLAM implementation using the extracted features from the previous processes.

3.1 Vision Process

Our goal is to extract vertical segments for a real time vision system on a small robot. Although *general purpose* edge detectors exist, and we implement several kinds by ourselves (Cabrol et al., 2005), they are not optimal in our particular case.

If we refer to the quicker general purpose method proposed by Kirsh, the use of the horizontal mask which detects horizontal gradient ie. local vertical edge, is sufficient. This simple remark allows to divide by more than four (one mask compared to four masks computation and the selection) the required computing time.

In the same manner all the following steps: thinning, closing, linking, and polygonal approximation are simplified (Nachar et al., 2014), and could be run faster:

- for the thinning step: only the horizontal left neighbor pixel is considered;
- for the closing step: only the one vertical neighbor, depending on the direction of the edge is recursively followed;
- for the polygonal approximation: this step is wholly simplified, because only vertical segments are taken into account. There is only one vertical segment by edge, so there is no need to compute a distance between the edge and the segment in order to cut the edge into several segments constituting the polygonal line.

The adaptation from B&W to RGB edge segmentation which is not available on OpenCV is trivial. However, there are in images a lot of chrominance edges, that is to say edges between regions from different colors with the same luminance, which are impossible to extract using B&W edge segmentations.

Starting from the following observation, a chrominance edge is marked in at least one of the three component (Red, Green or Blue) and on each pixel three gradient's magnitudes are computed: one for each component: $||\overrightarrow{G_R}||$, $||\overrightarrow{G_G}||$, and $||\overrightarrow{G_B}||$. Then, the magnitude of the color gradient is obtained:

$$||\overrightarrow{G_C}|| = max||\overrightarrow{G_R}||, ||\overrightarrow{G_G}||, ||\overrightarrow{G_B}||$$

The color gradient replaces the B&W (or luminance) gradient for the following steps.

The proposed optimization for detecting vertical edges (only) is algorithmic and can be implemented either in CPU or GPU. We implemented the optimized version of gradient computation and edges thinning steps on CPU under the SPMD (Simple Program Multiple Data) programming model. The image is divided in several adjacent strips and each is given to a CPU core. We are going to implement this on OpenCL using a RaspberryPi's GPU.

3.2 Lidar Process and Fusion

In this section, we will detail the lines extraction from lidar's data and their fusion with features previously extracted from the image.

3.2.1 Previous Work

In a former work, we applied Wall-Danielsson to the lidar pointcloud (Burtin et al., 2018). This method, originally used in the vision field, was found to be

(a) Indoor environment

(b) Polygonal approximation

Figure 3: Results of indoor polygonal approximation using a UTM-30LX Hokuyo lidar.

efficient at segmenting lidar data very fast and accurately because lidar data are represented as linked edge points, result from the edge linking step. The result of this segmentation is a polygonal approximation of the environment around the lidar sensor (Figure 3).

This provides us an approximation of a solid shape representing the environment around. The solid shape can be transformed with translation and rotation to perform prediction of the would-be measured distance in a certain amount of time with a given evolution of the robot.

3.2.2 Follow Up

Those lines computed previously in the polygonal approximation exist in the 2D plane defined by the lidar's lasers. Therefore, we can compute the coordinates of these lines in the camera frame with the extrinsic parameters (homogeneous transformation matrix between lidar and camera frames).

The image process provides us vertical lines in the focal plane of the camera (3.1). We can compute from each line a 3D plane (CDE) (cf. Figure: 2) composed of the line segment (DE) and the focal point of the camera (C). These three points describe a unique plane (CDE) and we can compute its cartesian coordinates:

$$(CDE): a \cdot x + b \cdot y + c \cdot z + d = 0 \tag{1}$$

The objective is to compute the intersection between a 3D plane and a 3D line extracted from the camera and lidar data. This is basic geometry, we solve the following system:

$$\begin{cases} x_P = x_A + k \cdot (x_B - x_A) \\ y_P = y_A + k \cdot (y_B - y_A) \\ z_P = z_A + k \cdot (z_B - z_A) \\ x_P \cdot a + y_P \cdot b + z_P \cdot c = -d \end{cases} \tag{2}$$

We have the points $A = (x_A, y_A, z_A)$ and $B = (x_B, y_B, z_B)$, end of each sides of the lidar segment and describing the line (L).

We solve the system to find the point $P = (x_P, y_P, z_P)$.

The solution is assured to be unique and existing because (AB) is not coplanar nor collinear with (CDE) plane.

It's important to note that points A and B are projected in the camera frame at the exact moment the image is taken. Because the lidar and camera have different frame rates, data aren't synchronized and are generated at different moments.

To tackle this issue, we apply the method previously explained, composed of two transformations:

1. The prediction of the would-be lidar's measure, considering the current velocities and the time step between the lidar and the camera data;
2. The rigid transformation between lidar and camera frame;

3.3 Localization using a SLAM Method

The extracted features are 3D points, but with our hypothesis of planar environment we can make a 2D assumption. 3D features become 2D and we can define them in the camera frame with cartesian (x_i, y_i) or polar coordinates.

We decided to implement a SLAM system using an extended Kalman filter (Kalman, 1960) with the observations from both the camera and lidar using the cartesian coordinates.

The estimation of the state vector, including the 2D pose $(\hat{x}_k, \hat{y}_k, \hat{\alpha}_k)$ and the "n" features is $3 + 2 \times n$ long:

$$\hat{\mathbf{X}}_k = [\hat{x}_k, \hat{y}_k, \hat{\alpha}_k, \hat{x}_{1_k}, \hat{y}_{1_k}, \cdots, \hat{x}_{n_k}, \hat{y}_{n_k}] \tag{3}$$

and the measurement vector, issued by the features in polar coordinates:

$$\mathbf{z}_{i_k} = \begin{cases} \rho_{i_k} = \sqrt{(x_{i_k} - x_k)^2 + (y_{i_k} - y_k)^2} \\ \theta_{i_k} = \arctan(\dfrac{y_{i_k} - y_k}{x_{i_k} - x_k}) - \alpha_k \end{cases} \tag{4}$$

Our evolution model estimates the pose of the robot at the next step with the evolution function $\mathbf{f}$ taking $\hat{\mathbf{X}}_k$, the state vector, and $\hat{\mathbf{u}}_k$, the command applied to the robot, as parameters:

$$\mathbf{X}_{k+1} = \mathbf{f}(\mathbf{X}_k, \mathbf{u}_k) + \mathbf{q}_k \tag{5}$$

$\mathbf{q}_k$ is a Gaussian, white noise with zero-mean, representative of the evolution noise.
The four steps of the Kalman algorithm are: Prediction, Observation, Innovation and Update.

Prediction.
We predict the state vector $(\hat{\mathbf{X}}_{k+1,k})$ at step $k+1$ with the evolution function. The covariance matrix associated to the prediction $(\mathbf{P}_{k+1,k})$ is also computed:

$$\mathbf{P}_{k+1,k} = \mathbf{F}_{x_k} \mathbf{P}_{k,k} \mathbf{F}_{x_k}^T + \mathbf{F}_{v_k} \mathbf{V}_{k,k} \mathbf{F}_{v_k}^T + \mathbf{Q}_k \tag{6}$$

while $\mathbf{F}_{x_k}$ and $\mathbf{F}_{v_k}$ are jacobians such as:

$$\begin{cases} \mathbf{F}_{x_k} = \dfrac{\partial \mathbf{f}}{\partial \hat{\mathbf{X}}_{k,k}} \\ \mathbf{F}_{v_k} = \dfrac{\partial \mathbf{f}}{\partial \mathbf{u}_k} \end{cases} \tag{7}$$

$\mathbf{V}_{k,k}$ is the noise of the command (Gaussian, white and with zero-mean).
With the predicted state, we compute the observation estimates:

$$\mathbf{z}_{k_{estimate}} = \mathbf{h}(\mathbf{X}_{k+1,k}) \tag{8}$$

Observation.
In this step, we apply the previous method explained and obtain the observation vector: $\mathbf{z}_{k_{observed}}$.

We match the observed values with the estimated ones using the Mahalanobis distance (chi-square) and RGB horizontal gradient. It's a two steps validation: first we reduce the area of research using the uncertainty of the feature and, in case of indeterminate corresponding to multiple features in the area, we distinguish between themselves using the horizontal RGB. This feature has been extracted from a vertical line, which is why the horizontal gradient is representative, salient and most likely unique in this restricted area.

Innovation.
The innovation vector is as follows:

$$\mathbf{I}_k = \mathbf{z}_{k_{observed}} - \mathbf{z}_{k_{estimate}} \tag{9}$$

The Jacobian $\mathbf{H}_{x_i}$ of the i^{th} observation is:

$$\mathbf{H}_{x_{i_k}} = \begin{bmatrix} \frac{-(x_{i_k}-x_k)}{r_i} & \frac{-(y_{i_k}-y_k)}{r_i} & 0 & \dots & \frac{(x_{i_k}-x_k)}{r_i} & \frac{(y_{i_k}-y_k)}{r_i} & \dots \\ \frac{(y_{i_k}-y_k)}{r_i^2} & \frac{-(x_{i_k}-x_k)}{r_i^2} & 1 & \dots & \frac{-(y_{i_k}-y_k)}{r_i^2} & \frac{(x_{i_k}-x_k)}{r_i^2} & \dots \end{bmatrix} \quad (10)$$

And: $r_i = \sqrt{(x_{i_k}-x_k)^2 + (y_{i_k}-y_k)^2}$.

Update.
The update step uses the innovation and the Kalman gain ($\mathbf{K}_k$) to update the predicted state and the new covariance matrix:

$$\begin{cases} \mathbf{K}_k = \mathbf{P}_{k+1,k} \cdot \mathbf{H}_x^T \cdot (\mathbf{H}_x \cdot \mathbf{P}_{k+1,k} \cdot \mathbf{H}_x^T)^{-1} \\ \hat{\mathbf{X}}_{k+1,k+1} = \hat{\mathbf{X}}_{k+1,k} + \mathbf{K}_k \cdot \mathbf{I}_k \\ \mathbf{P}_{k+1,k+1} = \mathbf{P}_{k+1,k} - \mathbf{K}_k \cdot \mathbf{H}_x \cdot \mathbf{P}_{k+1,k} \end{cases} \quad (11)$$

4 RESULTS

The previous approach have been tested with both virtual and real setups. We will detail both experiments in the following section.

4.1 Virtual Testing

One of the sides objectives in developing this localization method was the development, use and validation of an advanced robotic simulator. The concerned simulator is 4DV-Sim (http://www.4d-virtualiz.com/), developed by the company 4D-Virtualiz. Its development was initiated by two robotic PhD students (perception and command fields), that needed a powerful and capable simulator to speed up their work. It has become a professional tool dedicated to real-time robots simulation in an HIL (Hardware In the Loop) manner. The aim of this simulator is to replicate very accurately real environments, sensors and robots into the virtual world, including shadows, textures, georeferencing, communication protocols, disturbances, etc (Figure: 4).

This simulator offers sensors with diverse degrees of realism: it was possible during early prototyping to use a "perfect" LIDAR, providing perfects measured ranges, without any measurement noise. Later, when our algorithm obtained appropriate results, we increased the complexity by adding random Gaussian measurement noise. Finally, before field testing, we experimented the algorithm with the virtual replica of the real sensor. This virtual sensor has exactly the same characteristics than the real one: FOV, resolution, noise measurement, maximum range, frequency and even the communication protocol. The simulator is able to work in an hardware in the loop fashion

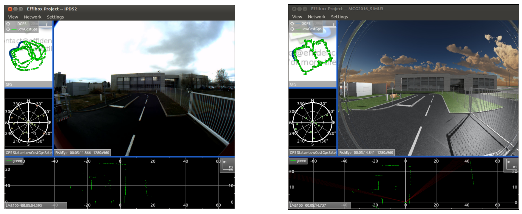

(a) Real sensors (b) Virtual sensors

Figure 4: Comparison of Camera, GPS ans LIDAR sensors between real data and data produced with the 4DV-Sim simulator.

which means that once the source code is validated with the virtual platform, it can be instantaneously carried to the real platform to be executed.

The use of a simulator also gives the opportunity to have exact repeatability to compare the results, access to ground truth and produce various datasets with different environments and robot set-ups, advantages we do not posses with experiments in real environment.

The simulated robot is a Dr. Robot Jaguar, virtually equipped with a URG-4LX Hokuyo lidar and a 640x480 global-shutter camera (pinhole model) (Figure: 5). The simulated lidar has the same parameters than the real URG-04LX (min angle, max angle, resolution, frequency, etc.) and the noise added to the measures is Gaussian distributed with parameters provided by the factory data-sheet.

Figure 5: Dr Robot Jaguar equipped with a URG-30LX lidar and RBG camera.

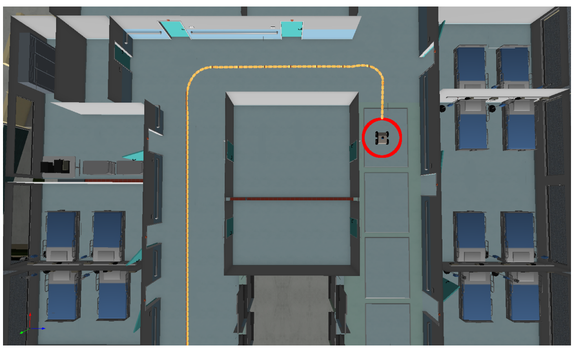

Figure 6: Simulated indoor environment containing the robot (red circle) and command trajectory (yellow).

The environment we used is a replica of a real

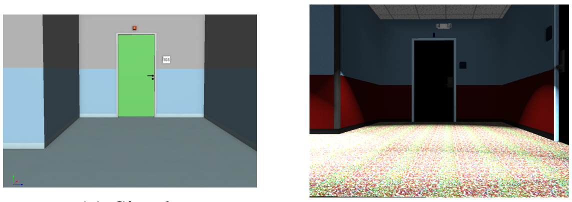

(a) Simple (b) Complex

Figure 7: Same environment, different complexity.

American hospital (Figure: 6). All doors, doorways, beds, hallways have the right scale and materials effects. In preliminary work, we used two different sets of textures and lighting effects to improve gradually the performance of the vision algorithm (Figure: 7).

4.1.1 Vision

In this section, two kinds of optimization for the Real Time Vision step will be presented, combined, and then discussed:

- of the algorithm: in order to detect vertical edges, only the horizontal gradient computation is required;
- of the implementation: the *data flow programming model* (Cabrol et al., 2005) is used, that is to say the computation of the pixel address is realized sequentially, pixel by pixel, by pointer incrementation.

A reference is proposed: it is a classical implementation of the Kirsh filter (Kirsch, 1971) in B&W and color RGB imagery. In this implementation, the computation of the pixel address is directly realized using one multiplication and one addition. The use of functions to access to the pixel value: `get_pixel()` and `put_pixel()` increases the computing time by 30%.

For each combination (algorithm / implementation) two computing time are presented:

- the low level processing, that is to say the gradient computation;
- the global time, where vertical segments are obtained.

One can notice that the low level processing is the most time consuming step, because the computations are performed on each pixel of the image. Consequently, the optimization of this step is the most important to realize, but it is also the most effective and easy to realize because of the regularity of the computations.

Time results are a mean using one hundred test RGB images (in `.ppm` format) given by our simulator on the hospital environment. As the content of the images is roughly similar, the computing time is quite constant. For more precision, the temporal measurement is realized on a loop of one hundred iterations.

Time results are measured on a PC HP Pro-book equipped of a processor Intel Core i5-630, at 2.4 GHz, with 16 Go of Memory. Images are in VGA format: 640 columns $\times$ 480 lines.

In B&W imagery, the Kirsh Algorithm takes 36 ms, and the global processing leading to the detection of the vertical segments 42,2 ms. The results for RGB color imagery are the following, in milliseconds:

Table 1: Average computation time in milliseconds.

Algo - Impl	No Opt	Optimized
Kirsh: 4 Masks	111 (93 %) - 119	20 (87 %) - 22,9
Horizontal Mask	30,2 (92 %) - 32,6	10,5 (77 %) - 13,6

In term of *Speed Up*, the results are the following:

Table 2: Acceleration depending on the method and the optimization.

Algo - Impl	No Opt	Optimized
Kirsh: 4 Masks	1	5,19
Horizontal Mask	3,65	8,75

As a conclusion, the increase of nearly factor 9 in computation time must be pointed out. It allows our vertical segment detection to run at video rate (ie. inferior to 40 ms) on one core. The use of less than 15 ms leaves the possibility to hook this segmentation part to other high level processing, and guaranty a latency time of less than a video frame. Using the SPMD programming model for the implementation of the gradient computation and edge thinning steps, a speed up of 3.8 is achieved using manual attribution on the 4 cores of the RaspberryPi against 2.7 using the Raspian load balancing.

4.1.2 Localization

We implemented the vertical detector presented previously and added the lidar data to obtain our 3D features. In order to reduce the computation time we limited the number of detected vertical lines and narrowed this to the lines around the horizon, we can observe the projection of the 3D extracted features from the previous image in cooperation with the lidar using camera intrinsic and extrinsic parameters (Figure: 8b).

In addition of the previous optimizations, we used regions of interest (ROI) to reduce the number of pixels processed during each steps. To define these ROI, we use the estimated position of the known feature in the image and defined the width of the bounding box using the uncertainty related to this feature with a minimal width of 10 pixels. The height of

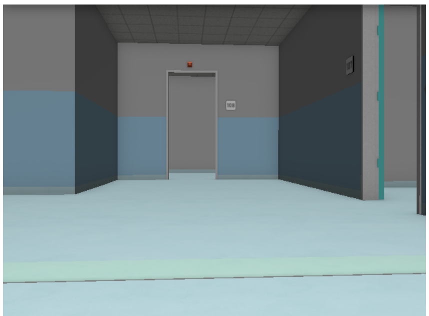

(a) Original image

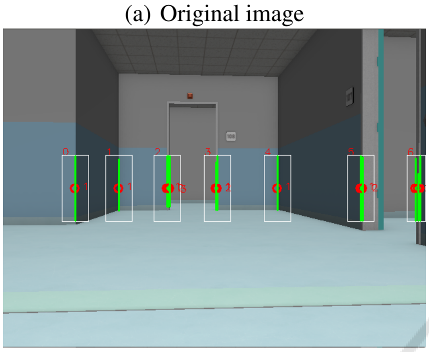

(b) Features

Figure 8: Use of ROI and the 2D features results in the SLAM map.

ROI's bounding box is fixed to 1/4 of the image. This is linked to the lidar's position: every "hit" from the lidar will be contained within the bounding box, whether the range is 0.5 or 30m (lidar's minimum and maximum range). The use of the ROI (Figure: 8b) is extended to the full width of the image when the algorithm looks for new features to add to the SLAM system. This allows a complete scan but has to be done at a lower frequency to save CPU-usage The average time needed to extract verticals in a ROI is 1.6623ms. Using a sparse SLAM system (even without multi-threading), we can reasonably track enough features in real time to feed a localization process.

We performed our experiment in the simulated environment using the described robot and setup; The result is displayed in the Figure: 9. The blue stars are the extracted and tracked features. One can recognize the shape of the building shown in top-view from Figure: 6. The green track is the ground truth from the simulator. The blue track is the estimated localization using only the odometry. We can observe the rapid drift of the odometry during turns and it's relative precision during forward motion. The black track is the estimated position of the robot using the kalman filter. The track is split in two parts, the first part has a very precise localization (an average 2cm error relatively to the ground truth), then a diverging part. The second part has an increasing error is due to a small error in heading at the moment of initialization of new landmarks when the robot faced the hallway. This is due to the lack of visual landmarks available in this part of the virtual map. This slight shift added a small angle that had repercussion on the next 25m of evolution to a final 0.3m error over a 40m trajectory. Blue stars are our observed landmarks and red one are registered in the map created. This conclude our virtual tests, considering that further tests should be on a real robot to confirm the results.

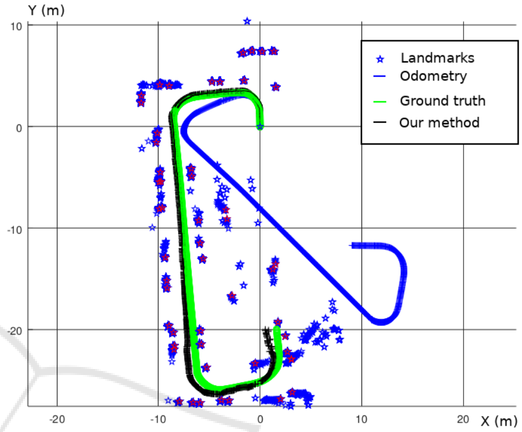

Figure 9: Localization results.

4.2 Real Experiments

Real experiment were conducted in the hallway of a public building. We used a Kobuki TurtleBot2 platform with an Hokuyo 04LX and an Intel Realsense D435 placed on the top of the robot. The environment we experienced in is about 40m long, having several patio doors with large panes, solid doors and shiny floor (Figure: 10).

(a) Real robot

(b) Hallway

Figure 10: Set-up and environment used for the experiment.

The RealSense sensor is used only to provide a global shutter 640x480 image, we didn't use the RGB-D feature because it did not provide depth information with sufficient range and precision. The corner seen on the left of the hallway is not seen at 3m (Figure: 11).

(a) Environment

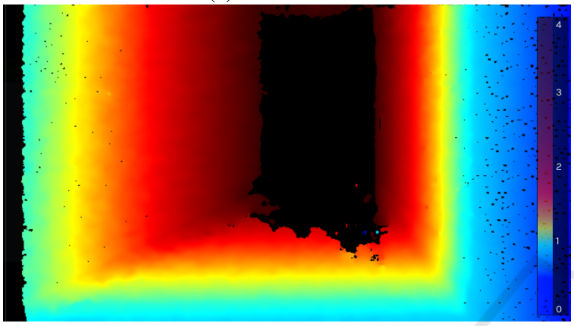
(b) Intel D435

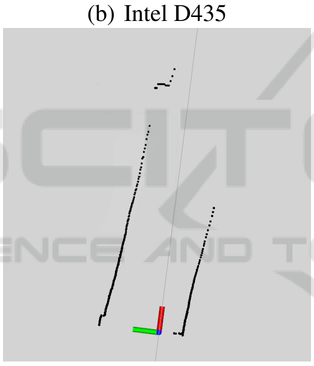
(c) Hokuyo 04-LX

Figure 11: Comparison of depth detection.

4.2.1 Localization

The real environment brought additional complexity to the sensors due to two facts: the large windows panes and the floor that reflects the environment. The first issue comes from the sun light that blinds the LIDAR sensor depending on the intensity of the rays. The second is brought by the clean plastic floor that create "false" verticals in the image by reflecting lights on the ceiling and doors. The first issue was solved by filtering the LIDAR data while the second one was only a matter of ROI focusing to exclude misleading verticals.

Our strong initial hypothesis, 2D movement and camera-lidar rig coplanar to the floor, is reasonable : even with small angular errors, we still manage to detect vertical lines in our image.

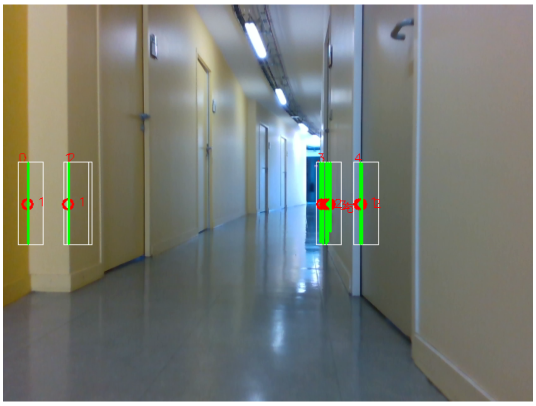
Figure 12: Detections with the real set-up.

As explained before, we do not have a proper ground-truth available for real experiment, thus we can't know the exact position of the robot during the experiment but we do have the 2D model of the building provided by the architects. This model have been produced using precise ($< 1cm$) measurement by professional surveyors, therefore, we can estimate the efficiency of the robot localization using the comparison between the landmarks registered by our system and the solid shape given by exact model (black shape in figure 13).

We compared the localization efficiency with another method: the canonical scan matcher (CSM) (Censi, 2008). We tried the ORB-Slam (Monocular) but the complex light rendered the initialization impossible. Since there is no loop closing in this hallway, the CSM should not have particular disadvantage.

On the Figure 13, we can observe the results of the different methods. The black trajectory is the lone odometry. The red one is the CSM result. The Blue stars are the landmarks registered by our method, and the trajectory is green. The odometry is outside the building frame but not that much, contrary to the virtual odometry, this one is more precise. This can be explained by the motion method of the robot: the virtual is a 4 wheeled robot and the TurtleBot is a 2 wheeled. The later present a reduced slippery during the turns, thus reducing the error on the odometry that made the assumption of slip-free rolling condition. The low range of the LIDAR and narrow FOV of the camera limits the number of landmarks available but the algorithm manages to detect several of them and successfully tracked, even with a complex lighting.

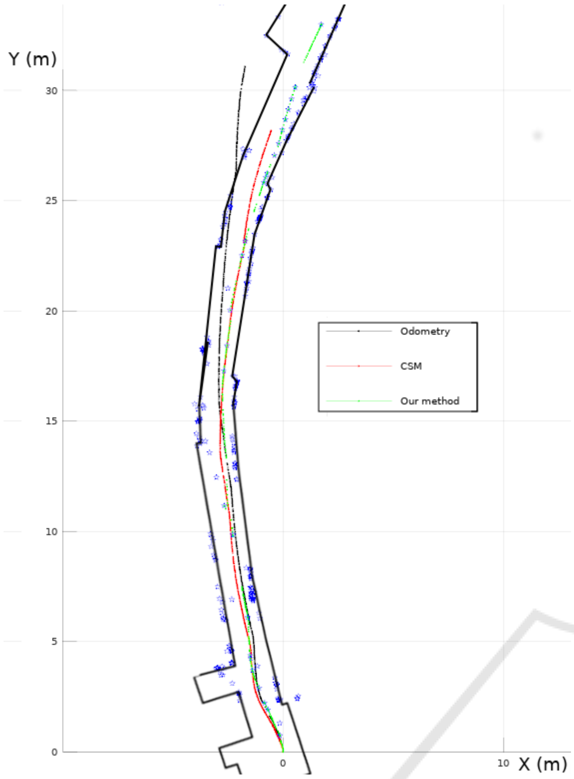

Figure 13: Localization results.

5 CONCLUSIONS

In this paper, we proposed an approach to extract features from both camera and lidar sensors while saving CPU-time. Upon this feature extractor, we built an extended Kalman filter to provide fast robot localization, re-using sensors data from others purposes. We evaluated the interest in focused images processing to reduce the computation time and observed a significant improvement, enough to process all features in real-time on a low grade computer. First, the localization method has been evaluated with an advanced robotic simulator and shown interesting results. Then the very same algorithm was used as-is later on a real platform, using the same sensor than the simulated ones. The landmarks localization in the experiment in the real hallway are conclusive regarding the 2D model of the building. We can reasonably state that the simulation was accurate enough to provide significant preliminary results. It allowed a real-time testing during the early development of the algorithm, having incremental complexity and access to ground truth. This helped significantly during the design of the system before using the real robot for final and real tests.

In future work, we will focus on improvement of the SLAM system to avoid heading shifts and include a loop-closing method to rectify the map. The use of RGB-D sensors to combine the image and depth with less calibration and more accurate results is an interesting perspective with more depth range.

ACKNOWLEDGEMENTS

This research was performed within the framework of a CIFRE grant (ANRT) for the doctoral work of G.Burtin at 4D-Virtualiz and LISV.

REFERENCES

Asvadi, A., Girao, P., Peixoto, P., and Nunes, U. (2016). 3d object tracking using rgb and lidar data. In *Intelligent Transportation Systems (ITSC), 2016 IEEE 19th International Conference on*, pages 1255–1260. IEEE.

Bekris, K. E., Glick, M., and Kavraki, L. E. (2006). Evaluation of algorithms for bearing-only slam. In *Robotics and Automation, 2006. ICRA 2006. Proceedings 2006 IEEE International Conference on*, pages 1937–1943. IEEE.

Burtin, G., Bonnin, P., and Malartre, F. (2018). Vision based lidar segmentation for accelerated scan matching. In *Journal of Communications*, volume 13, pages 139–144.

Burtin, G., Malartre, F., and Chapuis, R. (2016). Reducing the implementation uncertainty using an advanced robotic simulator.

Cabrol, A., P.Bonnin, V.Hugel, K.Boucheffra, and P.Blazevic (2005). Temporal optimized edge segmentation for mobile robotics. *SPIE Optics Photonics, Application of Digital Image Processing XXVIII, July 31st- August 4th 2005, San Diego, California, USA*.

Canny, J. (1983). Finding edges and lines in images. *MIT AI Lab Tech Report TR-720*.

Censi, A. (2008). An ICP variant using a point-to-line metric. In *Proceedings of the IEEE International Conference on Robotics and Automation (ICRA)*, Pasadena, CA.

Choi, Y.-H., Lee, T.-K., and Oh, S.-Y. (2008). A line feature based slam with low grade range sensors using geometric constraints and active exploration for mobile robot. *Autonomous Robots*, 24(1):13–27.

De Silva, V., Roche, J., and Kondoz, A. (2018). Robust fusion of lidar and wide-angle camera data for autonomous mobile robots. *Sensors*, 18(8):2730.

Deriche, R. (1987). Using canny's criteria to derive a recursively implemented optimal edge detector. *International Journal of Computer Vision, 167-187*.

Durrant-Whyte, H. and Bailey, T. (2006). Simultaneous localization and mapping: part i. *IEEE robotics & automation magazine*, 13(2):99–110.

Engel, J., Schöps, T., and Cremers, D. (2014). Lsd-slam: Large-scale direct monocular slam. In *European Conference on Computer Vision*, pages 834–849. Springer.

Engelhard, N., Endres, F., Hess, J., Sturm, J., and Burgard, W. (2011). Real-time 3d visual slam with a hand-held rgb-d camera. In *Proc. of the RGB-D Workshop on 3D Perception in Robotics at the European Robotics Forum, Vasteras, Sweden*, volume 180, pages 1–15.

Huang, H. (2008). *Bearing-only SLAM : a vision-based navigation system for autonomous robots*. PhD thesis, Queensland University of Technology.

Kalman, R. E. (1960). A new approach to linear filtering and prediction problems. *Transactions of the ASME–Journal of Basic Engineering*, 82(Series D):35–45.

Kirsch, R. (1971). Computer determination of the constituent structure of bio1ogical images. *Computers and Biomedical Research 4, 315-328*.

Lemaire, T. and Lacroix, S. (2007). Monocular-vision based slam using line segments. In *Robotics and Automation, 2007 IEEE International Conference on*, pages 2791–2796. IEEE.

Micusik, B. and Wildenauer, H. (2015). Descriptor free visual indoor localization with line segments. In *Proceedings of the IEEE Conference on Computer Vision and Pattern Recognition*, pages 3165–3173.

Mur-Artal, R., Montiel, J. M. M., and Tardos, J. D. (2015). Orb-slam: a versatile and accurate monocular slam system. *IEEE Transactions on Robotics*, 31(5):1147–1163.

Nachar, R., Inaty, E., Bonnin, P., and Alayli, Y. (2014). Polygonal approximation of an object contour by detecting edge dominant corners using iterative corner suppression. *VISAPP International Conference on Computer Vision Theory and Applications, pp 247-256, Jan 2014, Lisbon, Portugal*.

Newcombe, R. A., Lovegrove, S. J., and Davison, A. J. (2011). Dtam: Dense tracking and mapping in real-time. In *Computer Vision (ICCV), 2011 IEEE International Conference on*, pages 2320–2327. IEEE.

Premebida, C., Monteiro, G., Nunes, U., and Peixoto, P. (2007). A lidar and vision-based approach for pedestrian and vehicle detection and tracking. *rn*, 10:2.

Prewitt, J. (1970). Object enhacement and extraction. *Picture processing and Psychopictorics, BS. Lipking and A.Rosenfield ed, Academic Press*.

Pumarola, A., Vakhitov, A., Agudo, A., Sanfeliu, A., and Moreno-Noguer, F. (2017). Pl-slam: Real-time monocular visual slam with points and lines. In *Robotics and Automation (ICRA), 2017 IEEE International Conference on*, pages 4503–4508. IEEE.

Roberts, L. (1965). Machine perception of 3d solids. *Optical & electro optical information processing, JP.Tipett and al., Cambridge, MIT Press*.

Roumeliotis, S. I. and Bekey, G. A. (2000). Segments: A layered, dual-kalman filter algorithm for indoor feature extraction. In *Intelligent Robots and Systems, 2000.(IROS 2000). Proceedings. 2000 IEEE/RSJ International Conference on*, volume 1, pages 454–461. IEEE.

Schramm, S., Rangel, J., and Kroll, A. (2018). Data fusion for 3d thermal imaging using depth and stereo camera for robust self-localization. In *Sensors Applications Symposium (SAS), 2018 IEEE*, pages 1–6. IEEE.

Sobel, I. (1978). Neighborhood coding of binary images for fast contour following and general binary array processing. *Computer Graphics and Image Processing vol 8,*.

Von Gioi, R. G., Jakubowicz, J., Morel, J.-M., and Randall, G. (2012). Lsd: a line segment detector. *Image Processing On Line*, 2:35–55.

Zuo, X., Xie, X., Liu, Y., and Huang, G. (2017). Robust visual slam with point and line features. *arXiv preprint arXiv:1711.08654*.